Relaxation matrix for symmetric tops with inversion symmetry: Line coupling and line mixing effects on NH_3 lines in the ν_4 band

Q. Ma,[1] C. Boulet,[2] and R. H. Tipping[3]
[1]*NASA/Goddard Institute for Space Studies and Department of Applied Physics and Applied Mathematics, Columbia University, 2880 Broadway, New York, New York 10025, USA*
[2]*Institut des Sciences Moléculaires d'Orsay (ISMO), CNRS, Univ. Paris-Sud, Université Paris-Saclay, Bât. 350, Campus d'Orsay F-91405, France*
[3]*Department of Physics and Astronomy, University of Alabama, Tuscaloosa, Alabama 35487-0324, USA*

(Received 25 January 2017; accepted 16 March 2017; published online 7 April 2017)

Line shape parameters including the half-widths and the off-diagonal elements of the relaxation matrix have been calculated for self-broadened NH_3 lines in the perpendicular ν_4 band. As in the pure rotational and the parallel ν_1 bands, the small inversion splitting in this band causes a complete failure of the isolated line approximation. As a result, one has to use formalisms not relying on this approximation. However, due to differences between parallel and perpendicular bands of NH_3, the applicability of the formalism used in our previous studies of the ν_1 band and other parallel bands must be carefully verified. We have found that, as long as potential models only contain components with $K_1 = K_2 = 0$, whose matrix elements require the selection rule $\Delta k = 0$, the formalism is applicable for the ν_4 band with some minor adjustments. Based on both theoretical considerations and results from numerical calculations, the non-diagonality of the relaxation matrices in all the ^{P}P, ^{R}P, ^{P}Q, ^{R}Q, ^{P}R, and ^{R}R branches is discussed. Theoretically calculated self-broadened half-widths are compared with measurements and the values listed in HITRAN 2012. With respect to line coupling effects, we have compared our calculated intra-doublet off-diagonal elements of the relaxation matrix with reliable measurements carried out in the ^{P}P branch where the spectral environment is favorable. The agreement is rather good since our results do well reproduce the observed k and j dependences of these elements, thus validating our formalism. *Published by AIP Publishing.* [http://dx.doi.org/10.1063/1.4979492]

I. INTRODUCTION

It is well known that the non-diagonality of the Liouville scattering operator $\hat{S}$ must be taken into account in line shape theories or calculations of spectroscopic parameters (half-widths, shifts, relaxation matrices, and Rosenkranz line mixing parameters).[1,2] Unfortunately, due to the use of the isolated line approximation, the non-diagonality of $\hat{S}$ has been neglected in the semi-classical Robert-Bonamy (RB) formalism.[3] In 2013, we have developed a new formalism which does not use this approximation and with which the uncertainties in calculated half-widths are reduced, but also the whole relaxation matrix W can be predicted thus enabling to address line mixing effects through, for instance, the first order Rosenkranz line mixing coefficients.[1,2] In more recent works (denoted as Papers I and II in the following),[4,5] the formalism has been extended to study symmetric tops with inversion symmetry and applied to self-broadened NH_3 lines in parallel bands.

It is expected that a small inversion splitting would cause a complete failure of the isolated line approximation. This implies that the RB formalism is not applicable for the ν_1 and pure rotational bands of NH_3. In fact, in comparison with those predicted with the RB formalism, our calculated self-broadened half-widths of NH_3 lines are significantly smaller and match measurements very well.[4] Furthermore, because the whole relaxation matrix can be computed, it becomes possible to calculate the shapes of the Q branch and of some R manifolds in the ν_1 band[5] where signatures of line mixing have been experimentally observed by Pine and Markov.[6] More explicitly, our theoretical calculations excellently reproduce the profiles measured by Pine and Markov in the R(j = 3, k) manifold and the Q branch region and reasonably well match the Rosenkranz parameters deduced from the fit of experimental profiles for the R(3,k) manifold.

A different situation occurs in the ν_2 and $2\nu_2$ bands of NH_3 where the inversion splitting increases very quickly as the quantum number ν_2 increases. In the ground and $\nu_1 = 1$ levels, the splitting is about 1 cm^{-1}. For the $\nu_2 = 1$ and $\nu_2 = 2$ levels, it is about 36 cm^{-1} and 284 cm^{-1}, respectively. Based on these numbers one expects, when compared with the ν_1 band, very weak the line coupling and line mixing effects in the ν_2 band and completely negligible ones in the $2\nu_2$ band. This expectation was confirmed by both our calculated half-widths and Rosenkranz coefficients.[7] For the former, differences between those calculated with and without considering line coupling are very small or even negligible. Meanwhile, the calculated Rosenkranz coefficients in the ν_2 band are two orders of magnitude smaller than in the ν_1 band. However, those measured by Aroui *et al.*[8] in the ν_2 and $2\nu_2$ bands are of the same order as those measured in the ν_1 band. On one hand, the inversion splitting is the main source responsible for line mixing and its value increases by 36 times from the ν_1 band to the ν_2 band. On the other hand, as a measure of line mixing effects, the Rosenkranz coefficients reported by Aroui *et al.* do not

significantly change. Thus, their measured results are, for us, difficult to understand. In order to clarify this issue, we have proposed to make some new specific measurements in the ν_2 band.[7]

For the ν_4 band with a small inversion splitting (around 1 cm^{-1}), one expects significant line coupling and line mixing effects as well. Based on our experience and knowledge from studies of other bands, we think that it is better to compare our theoretical results with measurements performed under favorable spectroscopic conditions. Fortunately, as demonstrated by Hadded *et al.*,[9] "cleaner" measurements of intra-doublets coupling elements are possible for some ^{P}P(j,k) doublets. Even at relatively high pressures, the spectral profile of one specific doublet remains relatively well separated from its adjacent neighbors. This enabled them to directly measure intra-doublet off-diagonal elements of the W matrix and, consequently, to address their k and j dependences. A comparison between reliable measured results and theoretical calculations would be a decisive test of the validity of our theory.

In the present study, we extend the method developed in Papers I and II to the ν_4 band which, with respect to parallel bands, has some new features. It is a perpendicular band where the degenerate ν_4 mode is excited and a vibrational angular momentum $l_4 = \pm 1$ is present. Due to these new features, one has to carefully verify the applicability of the formalism used in parallel bands and make the proper modifications. Once this is completed, the remaining work is somehow similar to that reported in these two papers.

The manuscript is arranged in the following way. In Sec. II, we outline a frame of the theory and address the main differences between the formalisms applicable for parallel and perpendicular bands. In Sec. III, we present our calculated half-widths of NH_3 lines in the ν_4 band. Detailed analyses explain the reductions of calculated half-widths resulting from considering line coupling in different branches. Because there is an intrinsic link between the half-width reduction and the non-diagonality of the relaxation matrix W, the conclusions drawn from the former are also applicable to the latter. In addition, comparisons of the calculated half-widths with measurements[8,9] and data listed in HITRAN 2012[10] are also presented. In Sec. IV, we report calculated W matrix elements and compare our results in the ^{P}P branch with other calculations and with measurements. Finally, the main conclusions of this study are presented in Sec. V.

II. THEORY

A. States of the NH_3 molecule in the 000^00^0 level and in the ν_1 and ν_2 levels

It is well known that the wave functions of a symmetric-top molecule $|jkm\rangle$ are defined by

$$|jkm\rangle = \sqrt{(2j+1)/8\pi^2} D^{j*}_{mk}(\alpha, \beta, \gamma), \quad (1)$$

where $D^{j}_{mk}(\alpha, \beta, \gamma)$ are rotation matrices and the asterisk denotes the complex conjugate. For the NH_3 molecule, in order to find a proper expression for its wave functions, one needs to simultaneously consider the nuclear spin part as well as the ro-vibrational part. Meanwhile, the total wave functions must be anti-symmetric under permutation operators acting on its three H atoms. Readers can find detailed discussions on this subject provided by Green.[11] For states in the 000^00^0 level as well as in the excited ν_1 and/or ν_2 levels, the parity adapted wave functions of NH_3 are defined by

$$|n\nu\varepsilon jkm\rangle = |n\rangle \otimes N_\varepsilon (|\nu jkm\rangle + \varepsilon |\nu j - km\rangle). \quad (2)$$

In the above expression, a part of the wave functions associated with the vibrational inversion motion is explicitly presented by $|n\rangle$ with two choices: the symmetric vibrational inversion motion "s" and anti-symmetric one "a." In addition, a short notation ν is used to represent all vibrational quantum numbers (i.e., $\nu_1, \nu_2, \nu_3 = l_3 = \nu_4 = l_4 = 0$). With respect to rotational wave functions, the quantum number k is here the absolute value of the projection of the angular momentum j on the principal axis of the molecule. In other words, k = 0, 1, ..., j. For the normalization number N_ε, its value is $N_\varepsilon = 1$ for k = 0, and $N_\varepsilon = 1/\sqrt{2}$ for $k \neq 0$. Concerning the index ε, its value depends on both k and $|n\rangle$. More specifically, for k = 0, $\varepsilon = 0$ and for $k \neq 0$, $\varepsilon = (-1)^{j+1}$ or $\varepsilon = (-1)^j$ corresponding to the "s" or "a" inversion status.

It is worth mentioning that, once the symmetry associated with the nuclear spin wave function has been taken into account, if one assumes that the intermolecular potential does not act on the nuclear spins, it is unnecessary to explicitly include the spin wave function in the equations. We here use this simplifying convention, as done in Papers I and II. With respect to the vibrational inversion part (i.e., $|n\rangle$), we will omit it in the equations when its explicit presence is unnecessary.

The present formalism does not consider the various intra-molecular coupling terms that exist between the NH_3 states.[12] This implies that the wave functions adopted here are the "zero-order" ones. Note that this approximation is not suitable if one wants to predict the energy levels with high accuracy (e.g., 0.005 cm^{-1} as required by databases). However, for the calculation of pressure broadened line shape parameters, an uncertainty around, roughly speaking, 1 cm^{-1} is tolerable. It turns out that for the vibrational levels considered here, simple models neglecting all the intra-molecular resonances can be used. In the present study, we have used a formula containing two sets of parameters associated with the "s" and "a" inversion symmetries[13] to calculate energies in the 000^00^0 level. Numerical tests have shown that, in most cases, the accuracy of the calculated energies is satisfactory unless their rotational quantum numbers are beyond a certain limit (for example, $j_{max} = 10$).

B. States of the NH_3 molecule in the 000^01^1 level

For states in the 000^01^1 level, because the vibrational angular momentum is excited ($l_4 = \pm 1$) and the Coriolis force partly removes the degeneracy, their wave functions have a new feature. In this case, one needs to explicitly include the value of l_4 in the wave functions. For simplifying notations, except for the ν_4 and l_4 quantum numbers, all the other vibrational numbers are removed. Then, the parity adapted wave functions are given by

$$|n\nu_4 l_4 \varepsilon jkm\rangle = |n\rangle \otimes N_\varepsilon (|\nu_4 l_4 jkm\rangle + \varepsilon |\nu_4 - l_4 j - km\rangle), \quad (3)$$

where $N_\varepsilon = 1/\sqrt{2}$ with, for the "s" symmetry, $\varepsilon = (-1)^j$ and for the "a" symmetry, $\varepsilon = (-1)^{j+1}$. We note that this definition is applicable for both $k = 0$ and $k \neq 0$.

Numerous intra-molecular resonances are present in the $000^0 1^1$ levels.[13,14] For example, there is a strong Coriolis interaction between the ν_4 states with the "a" symmetry and the $2\nu_2$ states with the "s" symmetry that can cause avoided crossings for states with high j values. As a result, simple formulas used to calculate energy levels do not yield reliable values. We thus retrieved the energy levels up to $j_{max} = 10$ from the data of NH_3 lines in the ν_4 band provided by HITRAN 2008.[15] For the missing values, we have retained those provided by Huang.[16]

Now that the wave functions of interest are known, we follow Ben-Reuven's conventions[17] and introduce a set of bases $|n_i \nu_i \varepsilon_i j_i k_i n_f \nu_f \varepsilon_f j_f k_f, JM_J\rangle\rangle$ in the linespace defined by

$$\left|n_i \nu_i \varepsilon_i j_i k_i n_f \nu_4 l_4 \varepsilon_f j_f k_f, JM_J\right\rangle\rangle = \sum_{m_i m_f} (-1)^{j_f - m_f} \times C\left(j_i j_f J, m_i - m_f M_J\right) \left|n_i \nu_i \varepsilon_i j_i k_i m_i n_f \nu_4 l_4 \varepsilon_f j_f k_f m_f\right\rangle\rangle, \quad (4)$$

where the $C(L_1 L_2 L, \mu_1 \mu_2 M)$ are Clebsch-Gordan coefficients.

C. Potential model

For systems consisting of two symmetric-top molecules, the potential can be expressed in terms of a spherical tensor expansion as[18]

$$V\left(\vec{R}(t)\right) = \sum_{L_1 K_1 L_2 K_2 L} U(L_1 L_2 L; K_1 K_2; R(t)) \times \sum_{\mu_1 \mu_2 M} C(L_1 L_2 L, \mu_1 \mu_2 M) \times D^{L_1 *}_{\mu_1 K_1}(\Omega_a) D^{L_2 *}_{\mu_2 K_2}(\Omega_b) Y^*_{LM}(\omega(t)). \quad (5)$$

The isotropic part of the potential corresponding to the $L_1 = K_1 = L_2 = K_2 = 0$ component is modeled by a 12-6 Lennard-Jones (LJ) with $\sigma_{LJ} = 3.018$ Å and $\varepsilon_{LJ} = 294.3$ K.[19] Since we assume that the isotropic potential does not depend on vibrational motions, the values of σ_{LJ} and ε_{LJ} are the same as those used in Papers I and II. With respect to the anisotropic part, we assume that it consists of the dipole-dipole (V_{dd}), dipole-quadrupole (V_{dq}), quadrupole-dipole (V_{qd}), and quadrupole-quadrupole (V_{qq}) components. Let us emphasize that, because the dipole and quadrupole moments of NH_3 lie along its symmetric axis, all these components are labeled by $K_1 = K_2 = 0$. It is also worth mentioning that it is the mean values of the dipole and quadrupole moments within the initial vibrational state and within the final one that appear in these potential components. Except for the dipole moment which has different values in the $000^0 0^0$ and $000^0 1^1$ levels (i.e., 1.4715 and 1.4554 D[20]), we neglect other vibrational dependences for these components.

Because the NH_3 molecule has a very large dipole moment and a significant quadrupole moment, we expect that the combination of the four leading multipole interactions is sufficient to represent the NH_3–NH_3 anisotropic potential well. In addition, we note that, among these components, the V_{dd} term is the dominant one. Finally, all the other molecular parameters used to calculate the S_1 terms are derived here as explained in Paper I, and the "exact" trajectory model governed by the isotropic LJ potential is used in the present study. More detailed descriptions on the treatment can be found in Paper I.

D. Expressions for potential matrix elements in the $000^0 0^0$ and $000^0 1^1$ levels

Once the potential model is chosen, we need to know whether the formalism developed for the parallel bands in Paper I can be directly used here or requires some modifications. In order to answer this question, one has to consider the differences between the parallel bands and the ν_4 band.

At the current approximation level, there is only one important difference resulting from adopting the wave functions of Eq. (3) to represent final states in the ν_4 band. Due to this change, a representation constructed from the final states changes as well. According to textbooks of quantum mechanics, matrices of operators could have different forms in different representations. Therefore, one has to check if changes of the expressions of the potential matrix are needed.

Keep in mind that all the components of the potential model selected in the present study are characterized by $K_1 = K_2 = 0$. With Eq. (5), it is obvious that the main part of the potential matrix elements consists of products of matrix elements of $Q_{L_1} D^{L_1 *}_{\mu_1 K_1 = 0}(\Omega_a)$ in the Hilbert space of the absorber molecule a and matrix elements of $Q_{L_2} D^{L_2 *}_{\mu_2 K_2 = 0}(\Omega_b)$ in the Hilbert space of the perturber molecule b. Here, Q_L represents the parts of operators only acting on vibrational states. Therefore, one can only focus attention on these two matrix elements. Let us compare, for instance, the formalisms for the ν_1 (parallel) and ν_4 (perpendicular) bands. The only possible change of expressions for the whole potential matrix results from a possible difference between the matrix elements of $Q_{L_1} D^{L_1 *}_{\mu_1 K_1 = 0}(\Omega_a)$ in the $100^0 0^0$ and the $000^0 1^1$ levels.

In the Appendix, we provide a detailed comparison between these two expressions. Thanks to the fact that the potential model retained has $K_1 = K_2 = 0$, we have found that the expression for the potential matrix in the $000^0 1^1$ level is identical to that in the $000^0 0^0$ level. Consequently, the expressions for the whole potential matrix and all other formulas developed in Paper I are applicable in the ν_4 band. However, note that the above conclusion is only valid for the current potential model. For potential models containing components with $K_1 \neq 0$, such as $K_1 = 3$, one should carefully recheck this conclusion before carrying out studies.

E. Transition selection rules and interaction selection rules

With our formalism, one has to distinguish two sets of selection rules. One is the dipole transition rules with which one determines allowed lines in specified bands. The other is the interaction selection rules applicable to matrix elements of the potential that appear in the expressions of the $S_{2,outer,i}$, $S_{2,outer,f}$, and $S_{2,middle}$ terms.

It is well known that, for parallel bands of NH_3 such as the ν_1 band, the dipole transition selection rules are $\Delta j = 0, \pm 1$; $\Delta k = 0$; and $s \leftarrow a$, $a \leftarrow s$. For perpendicular bands such as the ν_4 band, they are $\Delta j = 0, \pm 1$; $\Delta k = \pm 1$; and $s \leftarrow s$, $a \leftarrow a$.

With respect to the interaction selection rules, because we have verified the similarity of the expressions of the potential

matrices in different vibrational levels, one can conclude that the interaction selection rules applicable for the ν_4 band are the same as those for the pure rotational and the ν_1 bands. By looking at the expressions for the potential matrix elements given in terms of the D^P matrix (see Eq. (9) provided later), it is easy to derive the interaction selection rules. For L = 1 and K = 0, they are $\Delta j = 0, \pm 1$; $\Delta k = 0$; and s ← a, a ← s. For L = 2 and K = 0, one has $\Delta j = 0, \pm 1, \pm 2$; $\Delta k = 0$; and s ← s, a ← a.

F. Construction of sub-blocks in the linespace

We have only derived reliable energy levels in the $000^0 1^1$ level up to $j_{max} = 10$. Hence, since high levels of energy in this level are not available, we have to limit the NH_3 lines to be considered in the ν_4 band such that their j_i values are not beyond 8. By setting $j_{imax} = 8$, there are 410 allowed lines remaining and the size of the matrices in the linespace is 410×410.

As explained in Paper I, the non-diagonality of $S_{2,middle}$ is the only source responsible for line couplings between NH_3 lines. By applying the interaction selection rules with $L_1 = 1$ and $L_1 = 2$ derived from the expressions of the matrix elements of $S_{2,middle}$ given below by Eq. (6), one can easily determine whether two given lines are coupled or not and consequently divide the line coupling matrices into sub-blocks. The smaller the sizes of these blocks are, the easier to handle all of them. Thanks for $\Delta k = 0$ appearing in these interaction selection rules, the line coupling does not occur between two lines either whose initial k values are different or whose final k values are different. This implies that the 410 lines must be categorized by their initial and final k values. In Table I, we present a list of the sub-blocks labeled by values of k_i and Δk ($\equiv k_f - k_i$) and the numbers of lines in each of the sub-blocks. For later convenience, two sub-blocks with $k_i = 1$, $\Delta k = -1$ and $k_i = 0$ and $\Delta k = 1$ are labeled in the group B and the remaining sub-blocks are in the group A.

TABLE I. Sizes of sub-blocks in the linespace constructed by NH_3 lines in the ν_4 band.

k_i	0	1	2	3	4	5	6	7	8
$\Delta k = 1$	24[a]	42	36	30	24	18	12	6	2
$\Delta k = -1$	0	48[a]	42	36	30	24	18	12	6

[a]The sub-block is in the group B. All others are in the group A.

As shown in Table I, there are 17 sub-blocks and the largest one (i.e., $k_i = 1$ and $\Delta k = -1$) has a size of 48×48, thus well within the ability range of our diagonalization codes.

G. Matrix elements of the relaxation operator

In order to calculate the relaxation matrix, one needs to calculate matrix elements of $-iS_1 - S_2$ first. For this purpose, the expressions for S_1, $S_{2,outer,i}$, $S_{2,outer,f}$, and $S_{2,middle}$ are required. At this stage, note that the formalism can be written in the standard or the symmetrized forms.[2] In the present study, we follow the latter where the density matrix ρ is symmetrized. It is easy to switch to the standard form with a replacement of $\sqrt{\rho_{i_2}\rho_{i'_2}}$ appearing in the expressions for $S_{2,outer,i}$, $S_{2,outer,f}$, and $S_{2,middle}$ by ρ_{i2}. Readers can find these expressions and how to evaluate the two and one dimensional symmetric correlation functions and their Fourier transforms in Paper I. For simplicity, we only recall the expression for the off-diagonal matrix elements of $S^{i'f',if}_{2,middle}$ here, i.e.,

$$
\begin{aligned}
S^{i'f',if}_{2,middle}(r_c) = {} & 2\pi(-1)^{1+J}\delta_{\nu'_i\nu_i}\delta_{\nu_f\nu'_f}(-1)^{j_f+j'_f}\sqrt{(2j'_i+1)(2j'_f+1)(2j_i+1)(2j_f+1)}\sum_{L_1K_1K'_1L_2K_2K'_2}(-1)^{L_1}W\left(j'_ij'_fj_ij_f,JL_1\right) \\
& \times D^P\left(\varepsilon'_ij'_ik'_i,\varepsilon_ij_ik_i;L_1K_1\right)D^P\left(\varepsilon_fj_fk_f,\varepsilon'_fj'_fk'_f;L_1K'_1\right)\sum_{i_2i'_2}\sqrt{\rho_{i_2}\rho_{i'_2}}\,(2j_2+1)\left(2j'_2+1\right) \\
& \times D^P\left(\varepsilon'_2j'_2k'_2,\varepsilon_2j_2k_2;L_2K_2\right)D^P\left(\varepsilon_2j_2k_2,\varepsilon'_2j'_2k'_2;L_2K'_2\right)\mathbb{F}_{L_1K_1K'_1L_2K_2K'_2}\left(\frac{\omega_{i'i}+\omega_{f'f}}{2}+\omega_{i'_2i_2},\omega_{fi}-\omega_{f'i'}\right). \qquad (6)
\end{aligned}
$$

Once all the matrix elements of S_1 and S_2 are known, the remaining task is to calculate matrix elements of $\exp(-iS_1 - S_2)$. The method used here for this purpose consists of two procedures. First, to diagonalize the matrix $-iS_1 - S_2$. Then, based on its eigenvalues and right (or left) eigenvectors, one calculate $\exp(-iS_1 - S_2)$. A detailed formula and its explanation can be found in Paper I.

Finally, after the above procedures are completed, the relaxation matrix elements can be easily obtained from

$$
\begin{aligned}
W_{i'f',if} = {} & \frac{n_b\bar{v}}{2\pi c}\int_{r_{c,min}}^{+\infty}2\pi\left(b\frac{db}{dr_c}\right)dr_c \\
& \times\left\{\delta_{i'i}\delta_{f'f}-\left\langle\left\langle i'f'\left|e^{-iS_1(r_c)-S_2(r_c)}\right|if\right\rangle\right\rangle\right\}, \qquad (7)
\end{aligned}
$$

where n_b is the number density of the bath molecules, $\bar{v}$ is the mean relative speed, b is the impact parameter, and r_c is the closest distance for a given trajectory. We do not perform an average over the relative kinetic energy at this stage. Such an approximation is known to be valid for half-width calculations. For the off-diagonal elements of W, our numerical tests have also demonstrated its validity for the current NH_3–NH_3 system with a dominant dipole-dipole interaction.

H. Theoretical predictions

After verifying and outlining a framework of the formalism applicable to the ν_4 band, one can predict some of the basic features of results obtained later through numerical calculations. As shown in Eq. (6), the coupling between two

given lines is mainly determined by three factors. The first two are $\frac{\omega_{i'i}+\omega_{f'f}}{2}+\omega_{i'_2 i_2}$, called the energy gap, and $\omega_{fi}-\omega_{f'i'}$ called the frequency gap appearing in the 2-D Fourier transforms $\mathbb{F}_{L_1K_1K'_1L_2K_2K'_2}$. By analyzing profiles of $\mathbb{F}_{L_1K_1K'_1L_2K_2K'_2}$ (see Fig. 3 of Paper I), we know that the smaller these two gaps are, the larger the magnitude of $\mathbb{F}_{L_1K_1K'_1L_2K_2K'_2}$. For two lines within a specified doublet, the energy gap is mainly determined by an average of the splits between the initial states and between the final ones while the frequency gap is simply a difference between them. This implies that these two gaps are always small in the ν_4 band and their variations over different doublets are small as well. Based on these considerations, one can draw two conclusions. First of all, for the ν_4 band with its small doublet splitting, the intra-doublet coupling is much more important than the inter-doublet one. There are some exceptions for some Q lines in which the inter- and intra-doublet couplings are comparable that we will discuss later. Second, the effect of these two gaps on the k and j dependences of the intra-doublet coupling is small.

The third factor influencing line couplings is the coupling strength factor defined by

$$(-1)^{L_1}\sqrt{(2j'_i+1)(2j'_f+1)(2j_i+1)(2j_f+1)}W\left(j'_i j'_f j_i j_f, 1L_1\right) \times D^P\left(\varepsilon'_i j'_i k'_i, \varepsilon_i j_i k_i; L_1K_1\right) D^P\left(\varepsilon_f j_f k_f, \varepsilon'_f j'_f k'_f; L_1K'_1\right), \quad (8)$$

where an expression for the D^P matrix is given by

$$\begin{aligned} D^P(\varepsilon' j' k', \varepsilon j k; LK) = N_{\varepsilon'}N_{\varepsilon}(-1)^k\{&C\,(jj'L, -kk'K) \\ &+\varepsilon' C\,(jj'L, -k-k'K) \\ &+\varepsilon C\,(jj'L, kk'K) \\ &+\varepsilon\varepsilon' C\,(jj'L, k-k'K)\}. \end{aligned} \quad (9)$$

It is worth mentioning that Eqs. (8) and (9) are also applicable for states in the 000^01^1 level because their quantum numbers ν_4 and l_4 are not relevant to their derivations. As shown by Eq. (6), because contributions to $S_{2,\text{middle}}$ are proportional to this factor, it plays a more direct role. Given the fact that we now known that the two gaps do not play a major role, we expect that the intra-doublet coupling is mainly determined by the coupling strength factor.

The D^P matrix has several symmetry properties. The two important ones are a symmetry between K and −K and a symmetry when switching ε′j′k′ and εjk. For the case $k' \neq 0$ and $k \neq 0$, they are

$$D^P(\varepsilon' j' k', \varepsilon j k; L-K) = (-1)^{j+j'+L}\,\varepsilon'\varepsilon D^P(\varepsilon' j' k', \varepsilon j k; LK), \quad (10)$$

and

$$D^P(\varepsilon j k; \varepsilon' j' k'; LK) = (-1)^{j+j'+L+K}\varepsilon'\varepsilon D^P(\varepsilon' j' k', \varepsilon j k; LK). \quad (11)$$

For the other three cases of $k'=k=0$; $k'=0, k\neq 0$; $k'\neq 0, k=0$, one has to replace the factor ε′ε in Eqs. (10) and (11) by 1, ε, and ε′, respectively. Alternatively, one can replace ε′ε by $\delta_{\varepsilon'0}\delta_{\varepsilon 0} + \varepsilon'(1-\delta_{\varepsilon 0}) + \varepsilon(1-\delta_{\varepsilon'0}) + \varepsilon'\varepsilon(1-\delta_{\varepsilon 0})(1-\delta_{\varepsilon'0})$ to cover all four cases. In the present study, because all the potential components are associated with K = 0, Eq. (10) applicable for $k' \neq 0$ and $k \neq 0$ is simplified as

$$D^P(\varepsilon' j' k', \varepsilon j k; L0) = 0 \textit{ unless } \varepsilon'\varepsilon(-1)^{j+j'+L} = 1. \quad (12)$$

With these properties and other theoretical considerations, one can make several predictions before carrying out numerical calculations. First of all, the line coupling must be very weak or negligible for the two sub-blocks in the group B. For the sub-block with $k_i = 0$, it does not contain any doublets. As a result, the usually dominant intra-doublet coupling does not exist in this block at all.

For another sub-block in this group, it does consist of doublets. But, because $k_f = 0$ in the final states of its lines, contributions to the intra-doublet coupling from the V_{dd} and V_{dq} components are zero. The reason for this is in their coupling strength factor, the matrix element of $D^P\left(\varepsilon_f j_f 0, \varepsilon'_f j_f 0; 10\right)$ contains the Clebsch-Gordan coefficients $C(j_f\ j_f\ 1,\ 000) = 0$. In addition, one can show that the V_{qd} and V_{qq} components do not make contributions to the intra-doublet coupling at all. This general conclusion directly results from Eq. (12) because doublets are always associated with $k' \neq 0$ and $k \neq 0$ and the "unless" factor becomes $\varepsilon_s\varepsilon_a(-1)^{j+j+2} = \varepsilon_s\varepsilon_a = -1$. By applying this conclusion to doublets in this sub-block, one can conclude that the intra-doublet coupling must be zero.

Besides, there is an approximate rule applicable to calculated half-widths for two lines which have switched initial and final inversion symmetries. For example, one expects that those of the $s^PQ(j, k)$ and $a^PQ(j, k)$ are almost identical. It is easy to understand this approximate symmetry because within each of these doublets, differences only result from the inversion indices "s" and "a" and, in general, the doubling splits associated with their initial and that with their final states are small. Although these symmetry properties are approximate, one can use them as tools to check the consistency of calculated results and also that of measured data because significant violations represent red flags.

III. CALCULATED HALF-WIDTHS

A. Reduction of calculated half-widths due to line coupling

It is known for years that the RB formalism significantly overestimates the half-widths.[21–23] In our earlier works,[1,2,24–26] we have demonstrated that for various systems, getting rid of the isolated line approximation reduces the calculated half-widths and improves the agreement with measurements. More recently, we have shown that because the doublet splitting of NH_3 lines in the pure rotational and ν_1 bands is only around 1 cm^{-1}, the isolated line approximation completely breaks down there. Consequently, the RB formalism overestimates the half-widths by a great amount. For the ν_2 band with a 36 cm^{-1} doublet splitting, the overestimation becomes much less and for the $2\nu_2$ band with a 284 cm^{-1} splitting, it is fully negligible.[7] With respect to the ν_4 band whose splitting is at the same level as the ground and ν_1 bands, we expect that calculated half-widths with the RB formalism must contain large errors. Our calculations confirm this prediction, as shown below.

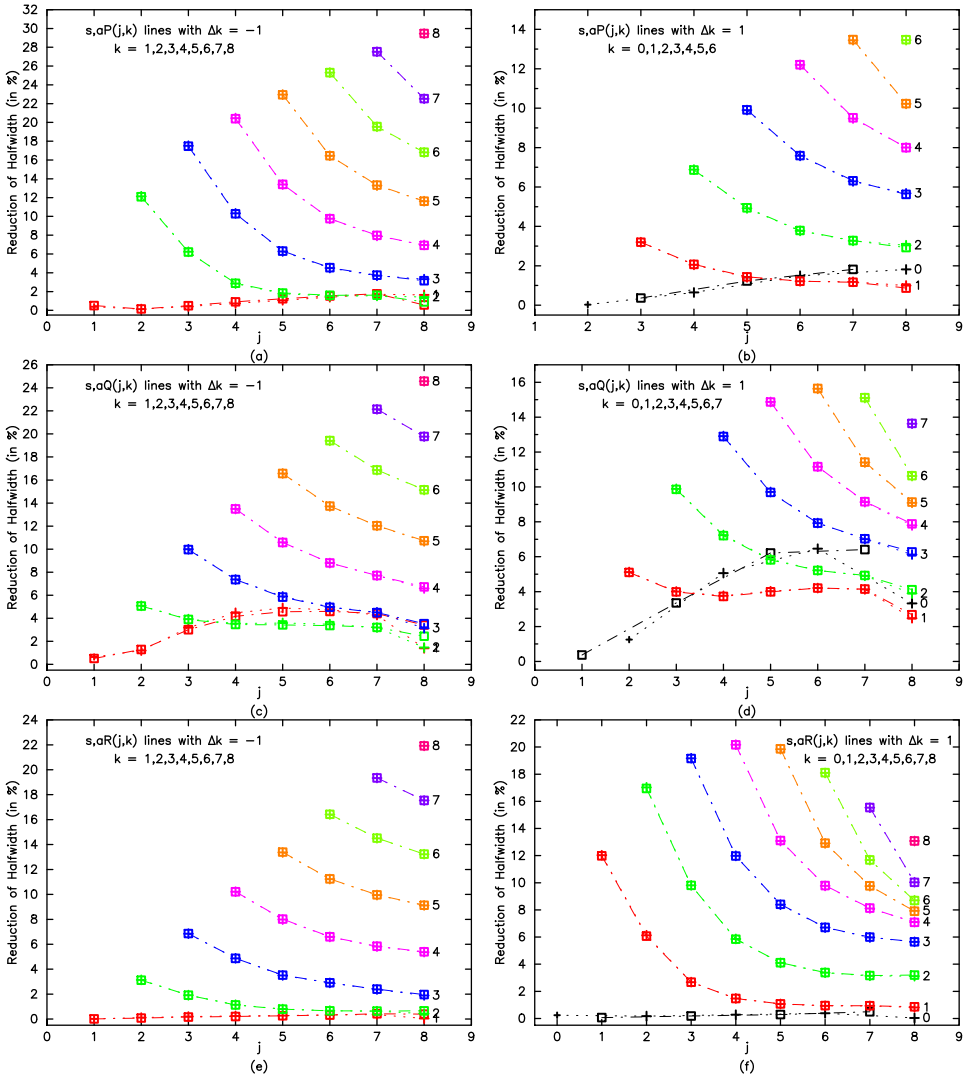

FIG. 1. Reductions of calculated half-widths due to considering the line coupling in the ^{P}P, ^{R}P, ^{P}Q, ^{R}Q, ^{P}R, and ^{R}R branches are presented in six plots labeled by (a)-(f). In the plots, transitions of s ← s and a ← a are distinguished by □ and +, respectively. In each of the branches, symbols in specified k blocks are given in the same color and connected by thin lines. Meanwhile, the sub-blocks are labeled by their k values at one of their far right members (i.e., j = 8) with the "a" symmetry.

We present reductions of the half-widths derived without and with the isolated line approximation for NH_3 lines in all six branches ^{P}P, ^{R}P, ^{P}Q, ^{R}Q, ^{P}R, and ^{R}R in Figs. 1(a)–1(f). Because both the reduction of calculated half-widths and the non-diagonality of the relaxation matrices result from the non-diagonality of the $S_{2,middle}$ operator, there must be an intrinsic link between them. Alternatively, in a sense, since the half-widths are diagonal elements of the relaxation matrix W, the reduced amount of the diagonal element due to removing the isolated line approximation must somehow go to the off-diagonal elements located at the corresponding column and row. Then, knowing what effective coupling mechanisms exist, one is able to determine not only how large the non-diagonality of W is but also, in most cases, to figure out which are the largest off-diagonal elements. Therefore, it is worthwhile to present a thorough discussion of these figures in Subsections III B and III C.

B. Non-diagonality of the relaxation matrices in the group A

We start our discussion for lines in the sub-blocks of group A. As shown in Figs. 1(a)–1(f), the reduction of the line widths varies from around 0% to 30% and strongly depends on k. The larger the k is, the larger the reduction. The reduction also varies with j with a maximum for the lowest j value (=k). Then, it decreases with a diminishing rate as j increases. By comparing the reductions in different branches, it appears that those in branches with $\Delta k = -1$ are larger than in those with $\Delta k = 1$. Among the three ones with $\Delta k = -1$, they are arranged as P, Q, and R from the largest to the smallest. However, this order is reversed for the three branches with $\Delta k = 1$.

First of all, let us recall some of the theoretical predictions made in Subsection II H. Because the doublet splits in the ν_4 band are small, the intra-doublet couplings are, in general, much more important than the inter-doublet ones. Second, for the intra-doublet couplings, the values of their two gaps remain small and only vary slightly, well within a few of cm^{-1}.

Then, we select the ^{R}Q branch as an example to go further in our analyses. In order to explain the k and j dependences of the half-width reductions shown in Fig. 1(d) more convincingly, we present the magnitudes of the coupling strength factor for the doublets with k = 1, 2, ..., 7 in Fig. 2(a). As can be seen, the most striking feature is the similarity of the dependences with those of the half-width reductions in Figs. 1(a)–1(c) and 1(e) for the ^{P}P, ^{R}P, ^{P}Q, and ^{P}R branches, except for the $^{P}Q(2,1)$ lines in Fig. 1(c) which will be discussed in Section IV B. However, the results in Fig. 2(a) and

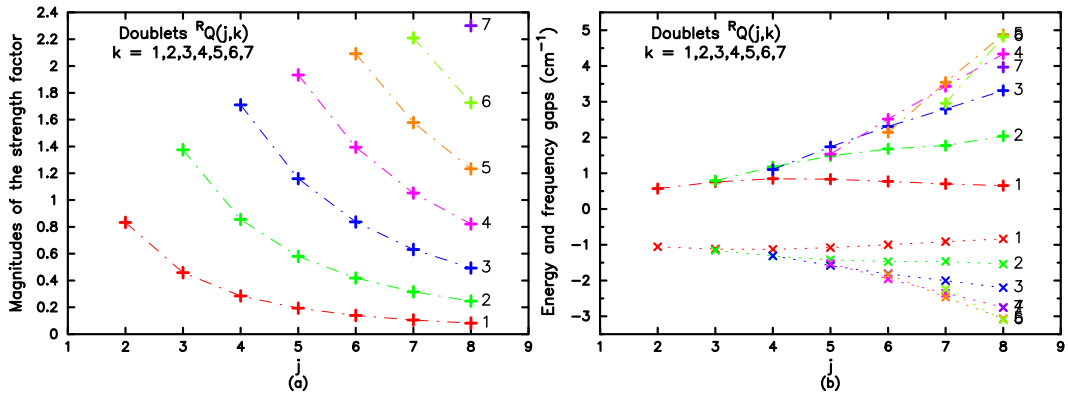

FIG. 2. Magnitudes of the coupling strength factor with $L_1 = 1$ and $K_1 = K_1' = 0$ for doublets with k = 1, 2, ..., 7 in the ^{R}Q branch are presented in Fig. 2(a). Meanwhile, values of the energy gap (×) and the frequency gap (+) are plotted in Fig. 2(b).

those in Fig. 1(d) look somehow similar but a significant difference between the variation patterns is observed. The relative similarity indicates that the coupling strength factor plays a major role in determining the k and j dependences. Meanwhile, the noticeable difference indicates that other sources also play a role. Looking at the difference more closely shows that large magnitudes associated with lines with high k values in Fig. 2(b) are reduced in Fig. 1(d). It turns out that it is the frequency gap and the energy gap that cause this diminution. In Fig. 2(b), we present values of these two gaps for the considered doublets. Note that the $\omega_{i_2' i_2}$ component is neglected in calculating the energy gap. This simplifying treatment is somehow justified (not always valid) by the fact that, as shown in Fig. 3 later, $\omega_{i_2' i_2} = 0$ occurs more often. As shown in Fig. 2(b), the frequency and energy gaps increase as k and j increase and the former is larger than the latter. Based on a typical profile of the leading 2-D Fourier transform $\mathbb{F}_{100100}$ presented in Fig. 3 of Paper I, its magnitude decreases very quickly as its two arguments go away from their central region. In addition, this Fourier transform is an even function of its two arguments. Roughly speaking, once the absolute values of its two arguments are greater than 3-4 cm^{-1}, its magnitude starts to fall down with an accelerative rate. Based on this fact, it is the frequency gap that plays the main role to reduce the enhancement of the coupling factor with the k value for the lines with $k \geq 3$ and $j \geq 7$. Meanwhile, reducing further the energy gap plays a minor role.

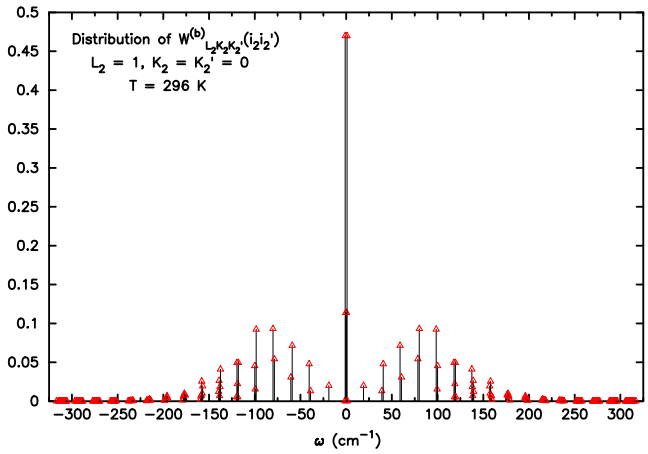

FIG. 3. The distribution of $W_{100}^{(b)}\left(i_2 i_2'\right)$ over $\omega_{i_2' i_2}$ with a resolution of 0.5 cm^{-1}.

It is worth mentioning that for all other 5 branches plotted in Fig. 1, except for a change of scale, the variations of the coupling strength factors are very similar. This common feature enables to explain the k and j dependence of the reduction for other branches. More explicitly, one can conclude that the coupling strength factor plays a dominant role in determining the reduction variation with k and j for the ^{P}P, ^{R}P, ^{P}Q, and ^{P}R branches because there are strong similarity between Figs. 1(a)–1(c), 1(e), and 2(a). Meanwhile, for the ^{R}R branch, just like the ^{R}Q branch discussed above, where large deviations between the two corresponding figures are observed, one expects the two gaps to play more significant roles there.

C. Non-diagonality of the relaxation matrices in the group B

We consider here lines in the sub-blocks of group B where the intra-doublet coupling does not exist. As shown in Figs. 1(a)–1(f), in comparison with lines in other sub-blocks, their half-width reductions are much smaller. Because a weak coupling means a small reduction and vice versa, this confirms the theoretical prediction for these two sub-blocks made in Subsection II H. However, their reductions are not zero, especially for the s,a^{P}Q(j,1), s,a^{R}Q(j,0), s,a^{P}P(j,1), and s,a^{R}P(j,0) lines where the maximum reduction reaches 6%. It turns out that, for these lines, the most important coupling happens between two lines whose j values differ by 1. In the following, we will select some samples and provide our theoretical explanations of their features.

For the sub-block with $k_i = 1$, $\Delta k = -1$, we list absolute values of the three coupling parameters for some pairs consisting of the lines s^{P}Q(j,1) and their nearby neighbours a^{P}Q(j ± 1,1) in Table II. As shown in the left side of Table II, their coupling strength factor (i.e., |St|) is pretty large and in favour of strong coupling. Meanwhile, the absolute values of the frequency gap (i.e., |ΔF|, in cm^{-1}) remain relatively small which is also in favour of strong coupling. However, their energy gaps without including $\omega_{i_2' i_2}$ (i.e., |ΔE|, in cm^{-1}) are very large. On first thought, such large |ΔE| may cause their coupling to be very small.

However, one has to remember that the contributions to the energy gap from the $\omega_{i_2' i_2}$ term have not been

TABLE II. Three coupling parameters for some pairs in two sub-blocks of the group B.

		$s^PQ(j,1)$				$s,a^RQ(j,0)$			
Factors	j′	j = 3	j = 4	j = 5	j = 6	s,j = 3	j = 4	j = 5	j = 6
|St|	j − 1	1.352	1.417	1.447	1.463	1.352	1.417	1.447	1.463
	j + 1	1.417	1.447	1.463	1.473	1.417	1.447	1.463	1.473
|ΔF|	j − 1	0.942	1.204	1.290	1.164	0.224	0.969	0.618	1.251
	j + 1	4.029	5.721	7.584	9.512	0.969	0.618	1.251	1.118
|ΔE|	j − 1	59.298	79.230	99.002	118.576	58.936	80.541	98.656	119.872
	j + 1	82.090	102.585	123.063	143.452	80.541	98.656	119.872	138.064

taken into account. As shown in Eq. (6), as a part of the argument $\frac{\omega_{i'i}+\omega_{j'f}}{2} + \omega_{i'_2 i_2}$ of $\mathbb{F}_{L_1K_1K'_1L_2K_2K'_2}$, this term occurs with weighting functions defined by

$$W^{(b)}_{L_2K_2K'_2}\left(i_2 i'_2\right) = \sum_{i_2 i'_2} \sqrt{\rho_{i_2}\rho_{i'_2}}\,(2j_2+1)\left(2j'_2+1\right) \times D^P\left(\varepsilon'_2 j'_2 k'_2, \varepsilon_2 j_2 k_2; L_2 K_2\right) \times D^P\left(\varepsilon_2 j_2 k_2, \varepsilon'_2 j'_2 k'_2; L_2 K'_2\right). \quad (13)$$

In Fig. 3, we present the leading weighting $W^{(b)}_{100}\left(i_2 i'_2\right)$ as a function of $\omega_{i'_2 i_2}$ [remind that its value divided by 3 (=2L$_2$ + 1) represents the probability with which a specified value of $\omega_{i'_2 i_2}$ occurs in Eq. (6)]. In this figure, the resolution is 0.5 cm^{-1}. In other words, the values within [ω_0 − 0.25, ω_0 + 0.25] are summed up and displayed at ω_0. As clearly seen, besides the most probable $\omega_{i'_2 i_2} \cong 0$, several other values (i.e., ±59, ±80, ±100, ...) also occur with non-negligible probabilities. For these values, perfect cancelations to the energy gaps listed in Table II become possible that lead to small values of the whole energy gap appearing as one argument of the Fourier transforms and consequently, relatively significant coupling. Careful readers may notice that there is no symmetry of listed two gaps between two pairs of {j, j − 1} and {j − 1, j}. The reason for this is that the inversion symmetries involved are not identical. For example, the coupling between $s^PQ(4,1)$ and $a^PQ(3,1)$ differs from that between $s^PQ(3,1)$ and $a^PQ(4,1)$.

Similarly, we select some pairs of lines in the sub-block with $k_i = 0$ and $\Delta k = 1$ and list their coupling parameters in the right side of Table II. The main mechanism responsible for their coupling is the same as that explained above for the sub-block with $k_i = 1$ and $\Delta k = -1$ and all analyses presented there are applicable here. We only note that there is a symmetry between two pairs of {j, j − 1} and {j − 1, j}. In the current case, the inversion symmetry is fixed with j. As a result, their "s" and "a" assignments are identical.

TABLE III. Self-broadening parameters (in 10^{-3} cm^{-1} atm^{-1}).

	Hadded *et al.*		Aroui *et al.*		Calculations	
Doublet	γ_s	γ_a	γ_s	γ_a	γ_s	γ_a
^{P}P(2,2)	581 (19)	584 (12)	581 (4)	590 (3)	593	592
^{P}P(3,1)	336 (3)	347 (4)	335 (2)	348 (1)	339	339
^{P}P(3,3)	620 (3)	616 (5)	612 (2)	626 (3)	616	616
^{P}P(4,3)	523 (4)	522 (9)	533 (2)	535 (3)	533	532
^{P}P(4,4)	607 (8)	619 (4)	604 (2)	617 (4)	625	624
^{P}P(5,3)	483 (4)	485 (3)	476 (4)	488 (3)	481	484
^{P}P(5,4)	552 (9)	544 (6)	553 (2)	545 (2)	560	562
^{P}P(5,5)	598 (7)	598 (11)	596 (3)	604 (4)	624	624
^{P}P(6,4)	496 (8)	486 (10)	501 (2)	497 (2)	507	508
^{P}P(6,5)	555 (8)	553 (6)	558 (2)	558 (2)	571	571
^{P}P(6,6)	595 (11)	609 (12)	594 (11)	600 (8)	619	619
^{P}P(7,6)	575 (15)	553 (7)	569 (3)	559 (4)	572	573
^{P}P(7,7)	592 (7)	587 (7)	612 (4)	592 (4)	613	614
^{P}P(8,7)	533 (22)	590 (11)	561 (3)	573 (3)	569	570
^{P}P(8,8)	576 (10)	582 (15)	586 (3)	596 (5)	608	608

D. Comparison with experimental data

As mentioned in the Introduction, the ^{P}P(j,k) doublets in the ν_4 band offer favorable conditions for reliable measurements of both line-broadening and line-mixing terms. In Table III, we present a comparison between our calculated half-widths of $s,a^PP(j,k)$ lines in the ν_4 band and the measured results by Hadded *et al.*[9] and by Aroui *et al.*[8] The agreements are good.

E. Comparisons between calculated half-widths and those listed in HITRAN 2012

In our previous studies of parallel bands of NH_3, we found that the agreements between our calculated half-widths and the values listed in HITRAN 2012 are not satisfactory and vary from reasonably good to poor among different branches. Our current study in the ν_4 band confirms this result. In general,

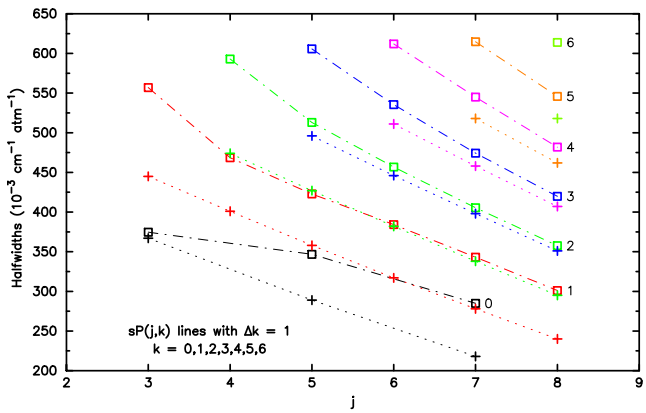

FIG. 4. A comparison between calculated half-widths of lines (□) in $s^RP(j,k)$ and HITRAN 2012 data (+).

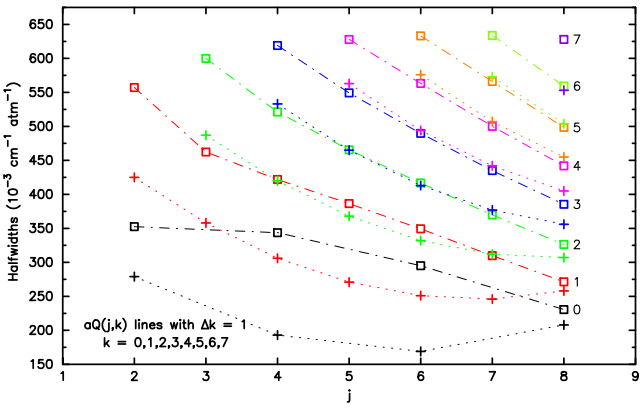

FIG. 5. The same as Fig. 4 except for lines in $a^{R}Q(j,k)$ branch.

TABLE IV. Measured half-widths (in units of 10^{-3} cm^{-1} atm^{-1}) for some doublets by Aroui *et al.*[8]

Doublet	$^{P}P(6,2)$	$^{P}P(7,4)$	$^{R}Q(2,1)$	$^{R}Q(3,1)$	$^{R}Q(3,2)$	$^{P}Q(4,4)$	$^{P}Q(5,5)$
γ_s	396	439	551	384	506	560	564
γ_a	363	474	491	418	561	651	676

the agreement is better for lines in ^{P}P, ^{P}Q, and ^{R}R branches than for the others. The worst situations occur for lines in ^{R}P and ^{R}Q branches, as shown in Figs. 4 and 5 for $a^{R}P(j,k)$ and $a^{R}Q(j,k)$ lines. Based on this, one can conclude that the empirical formulas[27] used to provide the HITRAN 2012 data have to be updated.

F. Approximate rule applicable to the half-widths of doublets

In Paper I, we have explained why the partners of a doublet (i.e., sP(j,k) and aP(j,k)) in the ν_1 band have almost equal half-widths. As shown by Table III, the situation is rather similar in the ν_4 band (and for the same reasons): differences between the calculated half-widths of the two lines with switched "s" and "a" are much less than 1%. Looking at the self-broadened half-width data in HITRAN 2012, we found that they follow this rule exactly. With this useful tool, we have also analyzed the measurements by Aroui *et al.*[8] As shown in Table III, they follow this rule reasonably well with differences below 4%. However, there are red flags elsewhere. In Table IV, we list some lines where differences between measured half-widths for doublet partners are beyond 10%, the largest 20% difference occurring for the doublet $s,a^{P}Q(5,5)$.

IV. CALCULATED RELAXATION MATRICES

A. Calculated W matrices for the sub-blocks in group A

The analysis of the k and j dependences of the reduction of the line widths provided first indications on the non-diagonality of the W matrices for the sub-blocks in group A. They are, of course, corroborated by the calculation of the corresponding W matrices. In Figs. 6(a) and 6(b), we present bar plots of calculated magnitudes of W elements in the $^{P}P(j,2)$ and $^{P}P(j,4)$ branches. The first branch with $k_i = 2$ contains 14 lines ordered as: $s^{P}P(2,2)$, $a^{P}P(2,2)$; $a^{P}Q(3,2)$, $s^{P}P(3,2)$; $s^{P}P(4,2)$, $a^{P}P(4,2)$; $a^{P}P(5,2)$, $s^{P}P(5,2)$; $s^{P}P(6,2)$, $a^{P}P(6,2)$; $a^{P}P(7,2)$, $s^{P}P(7,2)$; $s^{P}P(8,2)$, $a^{P}P(8,2)$ and the latter has 10 lines ordered as: $s^{P}P(4,4)$, $a^{P}P(4,4)$; $a^{P}P(5,4)$, $s^{P}P(5,4)$; ...; $s^{P}P(8,4)$, $a^{P}P(8,4)$. With these line order choices, the inter-doublet couplings allowed by the leading V_{dd} and V_{dq} interactions are kept out from the super-diagonal (i.e., $W_{l,l+1}$) and sub-diagonal (i.e., $W_{l+1,l}$) lines of the corresponding matrices. As a result, it becomes easier to identify the intra-doublet coupling elements.

Comparing Figs. 6(a) and 6(b) with the two curves for $s,a^{P}P(j,2)$ and $s,a^{P}P(j,4)$ shown in Fig. 1(a) shows that the k and j dependences of the reduction in Fig. 1(a) are similar to those in Fig. 6. The plots also clearly demonstrate that the intra-doublet elements are the largest off-diagonal elements and that the inter-doublet ones are almost negligible. We do not present similar plots for other branches, but readers can find all these calculated symmetrized relaxation matrix elements in the supplementary material.

Before completing our discussions on the W matrices in group A, one has to investigate the matrix associated with the $s,a^{P}Q(j,2)$ curve in Fig. 1(c). As mentioned previously, a subtle different behavior of this curve has caught our attention. In order to explain it, one needs to find out, besides the intra-doublet coupling which is the dominant mechanism responsible for other curves, if there is here another coupling mechanism. In Figs. 7(a) and 7(b), we present bar plots to show the intra- and inter-doublet off-diagonal elements of the $s,a^{P}Q(j,2)$ matrix constructed from the following 14 ordered lines: $s^{P}Q(2,2)$, $a^{P}Q(2,2)$; $a^{P}Q(3,2)$, $s^{P}Q(3,2)$; ...; $s^{P}P(8,2)$, $s^{P}P(8,2)$. As shown in the plots, the inter-doublet off-diagonal elements become significant starting from $j \geq 3$. They are

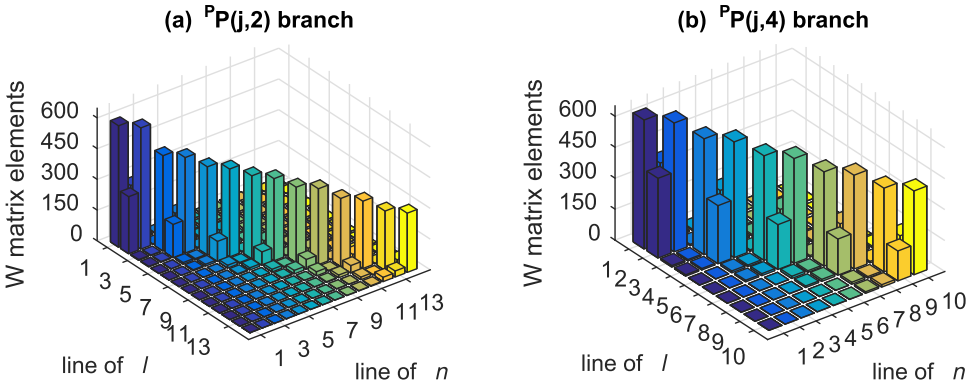

FIG. 6. Magnitudes of the relaxation matrix elements $W_{n,l}$ (10^{-3} cm^{-1} atm^{-1}) in two $s,a^{P}P(j,2)$ and $s,a^{P}P(j,4)$ branches containing 14 and 10 ordered NH_3 lines.

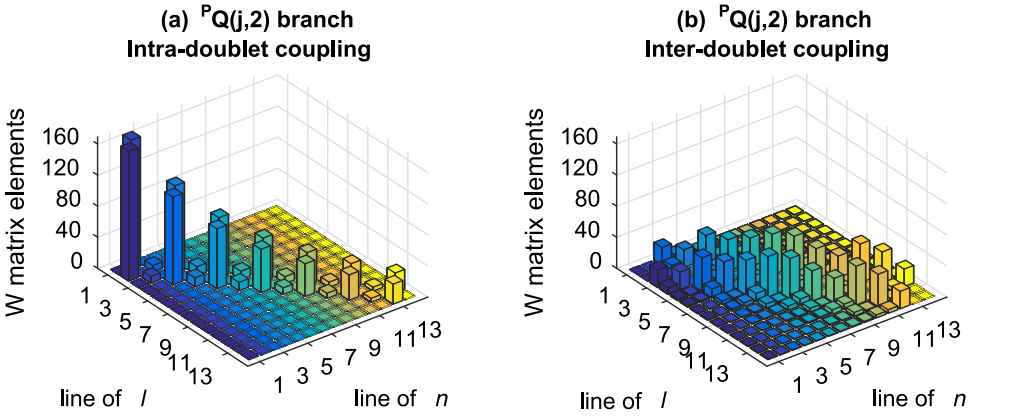

FIG. 7. Magnitudes of the off-diagonal elements $W_{n,l}$ (10^{-3} cm^{-1} atm^{-1}) in the s,a^{P}Q(j,2) branch containing 14 ordered lines of NH_3.

comparable with the intra-doublet ones for j ≥ 4 and become even larger for j ≥ 6. Thus, one can conclude that it is the inter-doublet coupling that affects the results for s,a^{P}Q(j,2) shown in Fig. 1(c). Now, the remaining question is as follows: why do significant inter-doublet couplings exist only for these Q lines, but not for their s,a^{P}P(j,2) and s,a^{P}R(j,2) partners. It is easy to find an answer by looking at their three coupling parameters. In general, the main features of the coupling parameters for the inter-doublet pairs are very similar to those listed in the left side of Table II, i.e., to have large values of the coupling strength factor, small frequency gaps (less than 1.5 cm^{-1}), and large energy gaps (without including $\omega_{i'_2 i_2}$). Based on the explanation for s^{P}Q(j,1) provided above, the set of coupling parameters for these Q lines give relatively large inter-doublet elements. With respect to their partners in the P and R branches, it turns out that their frequency gaps are always larger than 18 cm^{-1} which is enough to completely kill their couplings.

B. Calculated W matrices for the two sub-blocks in group B

Now, we present our calculated W matrices in the group B. As shown in Figs. 1(a)–1(f) and based on our discussions on these two sub-blocks in Section III A, two matrices constructed by lines in their Q branches have the largest non-diagonality and their coupling mechanisms have been explained. Here, we only present their bar plots to support our conclusions. First, we present the W matrix constructed from 10 ordered ^{P}Q(j,1) lines: s^{P}Q(1,1), a^{P}Q(1,1); a^{P}Q(2,1), s^{P}Q(2,1); ...; s^{P}Q(5,1), a^{P}Q(5,1) in Fig. 8(a). Note that the full size would be 16 × 16 matrix but, in order to improve visibility, we only plot the 10 × 10 part located at its left-upper corner. Readers need to pay extra attention on the elements along the super- and sub-diagonal lines because these zero-elements confirm that intra-doublet coupling does not exist here. The largest off-diagonal elements are located at the next super- and sub-diagonal lines. This confirms our prediction that the most effective coupling happens for two lines whose j values differ by 1.

Next, we present the W matrix constructed by 8 ^{R}Q(j,0) lines in another sub-block with k$_i$ = 0: s^{P}Q(1,0), a^{P}Q(2,0), s^{P}Q(3,0), a^{P}Q(4,0), s^{P}Q(5,0), a^{P}Q(6,0), s^{P}Q(7,0), and a^{P}Q(8,0) in Fig. 8(b) where its non-diagonality is clearly exhibited. Because there are no doublets here, the largest off-diagonal elements located at the super- and sub-diagonal lines result again from coupling between two lines whose j values differ by 1.

C. Comparison with measurements

As mentioned previously, we have used the symmetrized formalism to carry out numerical calculations. One can easily change the calculated relaxation matrices to their corresponding ones given in the standard form.[5] For intra-doublet off-diagonal elements W_{sa}, by applying a factor of $\exp\left(-\frac{\Delta E_{sa}}{2kT}\right)$ where ΔE_{sa} is the doublet splitting between their initial states, one can obtain values in the standard form from the symmetrized ones. Because $\Delta E_{sa} << 2kT$ at room temperature and in the ν_4 band, the values given in the two forms are almost identical. Based on this fact, we can directly compare our results with other experimental and theoretical values given in the standard form.

A comparison between some of the calculated off-diagonal elements of W in the ^{P}P branch and measured ones[8,9] is presented in Table V. We note that Aroui *et al.* have only provided their measured Rosenkranz mixing coefficients Y_l, but

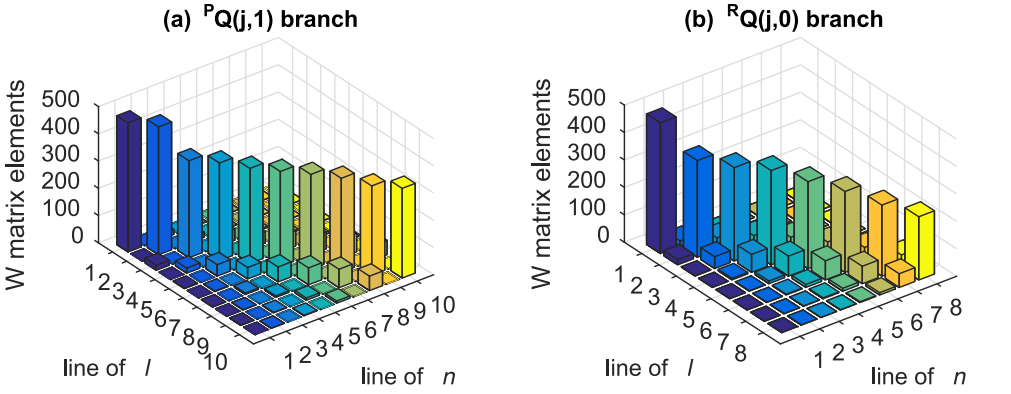

FIG. 8. Magnitudes of the relaxation matrix elements $W_{n,l}$ (10^{-3} cm^{-1} atm^{-1}) in the two sub-blocks of the group B. In Fig. 8(a), the matrix is constructed by 10 ordered Q lines in the s,aPQ(j,1) branch and in Fig. 8(b), it is by 8 Q lines in the ^{R}Q(j,0) branch.

TABLE V. Intra-doublet mixing elements of the relaxation matrix (in 10^{-3} cm^{-1} atm^{-1}). N/A means it is impossible to derive the value because Y_s and $|Y_a|$ differ too much.

Doublets	Hadded *et al.*[9]	Aroui *et al.*[8]	Present work
^{P}P(2,2)	−277(49)	−377(21)	−279
^{P}P(3,1)	−33(44)	N/A	0
^{P}P(3,3)	−385(19)	−392(6)	−351
^{P}P(4,3)	−260(4)	−268(12)	−235
^{P}P(4,4)	−349(26)	−415(14)	−386
^{P}P(5,3)	−243(16)	−190(18)	−166
^{P}P(5,4)	−263(12)	−306(17)	−282
^{P}P(5,5)	−450(12)	−500(19)	−411
^{P}P(6,4)	−280(68)	−321(22)	−217
^{P}P(6,5)	−305(11)	−326(12)	−318
^{P}P(6,6)	−441(14)	−458(13)	−431
^{P}P(7,6)	−404(27)	−384(14)	−349
^{P}P(7,7)	−484(15)	−537(11)	−448
^{P}P(8,7)	−148(106)	−403(24)	−375
^{P}P(8,8)	−498(54)	−596(13)	−461

no off-diagonal elements in this branch.[8] The corresponding values listed in Table V have thus been derived by us. Indeed, assuming $Y_s = -Y_a$ and introducing $\overline{Y} = (Y_s + |Y_a|)/2$, one can express the intra-doublet element as $W_{sa} = \bar{Y}\Delta F_{sa}/2$, where ΔF_{sa} is the frequency gap.

As shown in Table V, in general, the agreement, including the k and j dependences, is reasonably good. One of the Hadded's measured values[9] deserves to be pointed out. For the doublet ^{P}P(3,1), their measured value (i.e., 33(44)) is one order smaller than other values. As mentioned several times previously, our theoretical value is zero. By considering the large uncertainty attached to this measured value, the measurement supports our theory.

D. Comparison with other calculations

Recently, Starikov[28] has used the method developed by Cherkasov[29,30] to calculate some intra-doublet coupling elements of the W matrix. In Fig. 9, we present his calculated matrix elements associated with s,a^{P}P(j, k = j) lines together with our results and measured values.[9] As shown in the figure, both theoretical results exhibit a similar variation pattern as j varies. But, in comparison with measurements, the agreement reached by our results is better. We note that although the trajectory model adopted by Starikov in his calculations differs from ours, the effect of this difference is very small. Furthermore, the potential models used in both calculations, including the LJ parameters σ_{LJ} and ε_{LJ}, are identical. In our opinion, the improvement is mainly caused by an essential difference between the two methods. In both the formalisms, the Liouville scattering operator $\hat{S}$ is given by exponential forms which are however different. In the formalism of Cherkasov, the operator appearing in the exponential form for $\hat{S}$ depends on states of the bath molecule. As a result, he had to introduce an additional approximation to avoid diagonalizing huge matrices. With our method, the exponential form is obtained through the well-known cumulant expansion and the operators appearing there do not depend on bath states. Thus, one can accurately evaluate matrix elements of our exponential operator without any additional approximation.

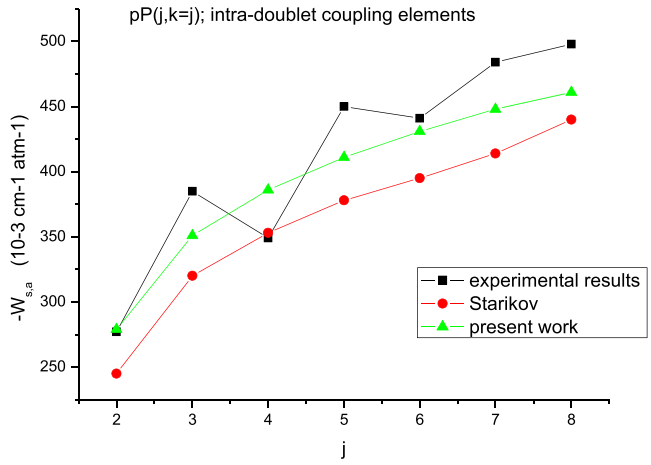

FIG. 9. Comparison between calculated and measured magnitudes of the intra-doublet elements $W_{s,a}$ for ^{P}P(j,k = j) doublets in the ν_4 band.

V. CONCLUSION

This work is our effort to verify the theoretical method presented in Paper I for the calculation of self-broadened half-widths and relaxation matrices of NH_3 lines. In order to meet requirements for the remote sensing inversion of tropospheric and planetary spectra, adding accurate line mixing parameters into NH_3 databases becomes necessary. Since reliable measurements of the line mixing parameters are very difficult to perform, validated theoretical calculations can provide some supports to achieve this goal.

Regarding theoretical calculations of the half-width of NH_3 lines, removing the isolated line approximation from the RB formalism has significantly improved the accuracy of calculated results both in parallel[4,7] and perpendicular (present work) bands. The smaller the inversion splitting is, the more this approximation breaks down. For the pure rotational, ν_1, and ν_4 bands where the splitting is very small, reductions of calculated half-widths resulting from removing this approximation can be very large (up to 30% in some cases). Meanwhile, the reduction significantly varies as k and j vary. In contrast, for the ν_2 band, its inversion splitting of 36 cm^{-1} results in very small or negligible reductions. Finally, thanks for having very strong long-range anisotropic interactions in the NH_3–NH_3 system where the current formalism can yield reliable theoretical results; our calculated half-widths are in good agreements with the available experimental data in all these bands.

Concerning the relaxation matrix, significant reductions of calculated half-widths directly indicate a strong non-diagonality. Fortunately, the ^{P}P(j,k) doublets in the ν_4 band are relatively well isolated and enable reliable measurements of the intra-doublet off-diagonal elements of the W matrix and consequently, to address their k and j dependences. For these doublets, our calculated W elements agree well with the measured values, including their k and j variation patterns.

Unfortunately, due to unfavorable spectral conditions, there are no other reliable measured data available in the

literature. In addition, there is no measurement to demonstrate the signatures of line mixing in the ν_4 band similar to that reported in the ν_1 band. In Paper II, we have shown that our formalism can successfully match the latter.

As a possible way to improve the quality of measured data for less favorable spectral regions, our suggestion is to impose some rules established from theoretical considerations while fitting measured spectra. With respect to refining our theoretical method, it would be interesting to see whether the strong intramolecular couplings (Coriolis, etc...) affect calculated results or not. In the present study, we have only adopted the 0-th order wave functions in which the mixture of the a-ν_4 and s-$2\nu_2$ states has been neglected. Finally, the present formalism may be extended to consider foreign-broadening cases (NH_3–N_2, NH_3–atoms, etc....) where some experiments have shown that line mixing effects differ significantly from those observed and calculated in the self-broadening case.[6,31]

SUPPLEMENTARY MATERIAL

See the supplementary material for all the calculated relaxation matrices in the ν_4 band.

ACKNOWLEDGMENTS

The authors are grateful to Dr. I. Kleiner for many stimulating and helpful discussions on the NH_3 spectroscopy and they would like also to thank Dr. X. Huang (NASA/Ames) and Dr. S. Yu (NASA/JPL) for helpful discussions on the energy levels of NH_3. We also thank Dr. J. M. Hartmann for greatly improving the manuscript. Two of the authors (Q. Ma and R. H. Tipping) acknowledge financial support from NSF under Grant No. 1501297. This research used resources of the National Research Scientific Computing Center, which is supported by the Office of Science of the U.S. Department of Energy under Contract No. DE-AC02-05CH11231.

APPENDIX: MATRIX ELEMENTS OF THE POTENTIAL OPERATOR IN THE 000^00^0 AND 000^01^1 LEVELS

In the following, we assume that the intermolecular potential model does not contain any components with $K_1 \neq 0$ or $K_2 \neq 0$. Without losing any generality, we consider a part of the potential operator in the Hilbert space of the absorber molecule a and assume that it consists of a product of Q_{L_1} and X where the former is the dipole operator μ_{10} with $L_1 = 1$ or the quadrupole operator Θ_{20} with $L_1 = 2$. Meanwhile, X is the rotational operator $D^{L_1*}_{\mu_1 K_1=0}(\Omega_a)$.

Let us derive expressions for potential matrices in the 000^00^0 level first. Keep in mind that because $K_1 = 0$, the rotational matrix elements of $\langle$j'k'm'|X|jkm$\rangle$ are zero unless $k' = k$. Then, we have

$$\begin{aligned}\langle n'v\varepsilon'j'k'm'|Q_{L_1}X|nv\varepsilon jkm\rangle &= \langle n'v|Q_{L_1}|nv\rangle N_{\varepsilon'}N_{\varepsilon}\left(\delta_{k'k}\langle j'k'm'|X|jkm\rangle + \varepsilon\delta_{k'-k}\langle j'k'm'|X|j-km\rangle\right.\\ &+ \left.\varepsilon'\delta_{-k'k}\langle j'-k'm'|X|jkm\rangle + \varepsilon'\varepsilon\delta_{-k'-k}\langle j'-k'm'|X|j-km\rangle\right)\\ &= \langle n'v|Q_{L_1}|nv\rangle \times N_{\varepsilon'}N_{\varepsilon}\delta_{k'k}\left(\langle j'k'm'|X|jkm\rangle + \varepsilon'\varepsilon\langle j'-k'm'|X|j-km\rangle\right). \qquad \text{(A1)}\end{aligned}$$

While deriving the last step we have used the fact that for $k' = k > 0$, $\delta_{k'-k} = \delta_{-k'k} = 0$ and for $k' = k = 0$, $\varepsilon' = \varepsilon = 0$. Thus, one can remove the second and third terms in the second line of Eq. (A1).

Then, we present the potential matrix elements in the 000^01^1 level as

$$\begin{aligned}\left\langle n'v_4l_4'\varepsilon'j'k'm'|Q_{L_1}X|nv_4l_4\varepsilon jkm\right\rangle &= N_{\varepsilon'}N_{\varepsilon}\left(\left\langle n'v_4l_4'|Q_{L_1}|nv_4l_4\right\rangle\delta_{k'k}\langle j'k'm'|X|jkm\rangle\right.\\ &+\varepsilon\left\langle n'v_4l_4'|Q_{L_1}|nv_4-l_4\right\rangle\delta_{k'-k}\langle j'k'm'|X|j-km\rangle\\ &+\varepsilon'\left\langle n'v_4-l_4'|Q_{L_1}|nv_4l_4\right\rangle\delta_{-k'k}\langle j'-k'm'|X|jkm\rangle\\ &+\left.\varepsilon'\varepsilon\left\langle n'v_4-l_4'|Q_{L_1}|nv_4-l_4\right\rangle\delta_{-k'-k}\langle j'-k'm'|X|j-km\rangle\right). \qquad \text{(A2)}\end{aligned}$$

Similarly, for $k' = k \neq 0$, the second and third terms of Eq. (A2) are zero. For $k' = k = 0$, the previous argument does not work because the definition of ε has been changed. However, for NH_3 states with $k = 0$ in the 000^01^1 level, their quantum number l_4 is fixed. In addition, because the operator Q_{L_1} does not change the vibrational angular motion, there is a Kronecker factor of $\delta_{l_4'-l_4}$ attached to these two terms that causes them to be zero again. Finally, based on the fact that $(\langle n'v_4l_4|Q_{L_1}|nv_4l_4\rangle = \langle n'v_4-l_4|Q_{L_1}|nv_4-l_4\rangle)$, we obtain

$$\left\langle n'v_4l_4'\varepsilon'j'k'm'|Q_{L_1}X|nv_4l_4\varepsilon jkm\right\rangle = \langle n'v_4l_4|Q_{L_1}|nv_4l_4\rangle N_{\varepsilon'}N_{\varepsilon}\delta_{k'k}\left(\langle j'k'm'|X|jkm\rangle + \varepsilon'\varepsilon\langle j'-k'm'|X|j-km\rangle\right). \qquad \text{(A3)}$$

By comparing Eqs. (A1) and (A3), it is obvious that their forms are identical. We note that the values of the dipole moment in the 000^00^0 and 000^01^1 levels (i.e., 1.4715 and 1.4554 D) come from $\langle n'v|Q_{L_1=1}|nv\rangle$ in Eq. (A1) and $\langle n'v_4l_4|Q_{L_1=1}|nv_4l_4\rangle$ in Eq. (A3), respectively.

[1]Q. Ma, C. Boulet, and R. H. Tipping, J. Chem. Phys. **139**, 034305 (2013).
[2]C. Boulet, Q. Ma, and F. Thibault, J. Chem. Phys. **140**, 084310 (2014).
[3]D. Robert and J. Bonamy, J. Phys. **40**, 0923 (1979).
[4]Q. Ma and C. Boulet, J. Chem. Phys. **144**, 224303 (2016).
[5]C. Boulet and Q. Ma, J. Chem. Phys. **144**, 224304 (2016).
[6]A. S. Pine and V. N. Markov, J. Mol. Spectrosc. **228**, 121 (2004).
[7]Q. Ma, C. Boulet, and R. H. Tipping, "Vibrational dependence of line coupling and line mixing in self-broadened parallel bands of NH_3," J. Quant. Spectrosc. Radiat. Transfer (published online).
[8]H. Aroui, H. Laribi, J. Orphal, and P. Chelin, J. Quant. Spectrosc. Radiat. Transfer **110**, 2037 (2009).
[9]S. Hadded, H. Aroui, J. Orphal, J. P. Bouanich, and J. M. Hartmann, J. Mol. Spectrosc. **210**, 275 (2001).
[10]L. S. Rothman *et al.*, J. Quant. Spectrosc. Radiat. Transfer **130**, 4 (2013).

[11]S. Green, J. Chem. Phys. **73**, 2740 (1980).
[12]S. Urban, J. Quant. Spectrosc. Radiat. Transfer **48**, 675 (1992).
[13]C. Cottaz, I. Kleiner, G. Tarrago, L. R. Brown, J. S. Margolis, R. L. Poynter, H. M. Pickett, T. Fouchet, P. Drossart, and E. Lellouch, J. Mol. Spectrosc. **203**, 285 (2000).
[14]S. Urban, V. Spirko, D. Papousek, R. S. McDowell, N. G. Nereson, S. P. Belov, L. I. Gershtein, A. V. Maslovskij, A. F. Krupnov, J. Curtis, and K. N. Rao, J. Mol. Spectrosc. **79**, 455 (1980).
[15]L. S. Rothman *et al.*, J. Quant. Spectrosc. Radiat. Transfer **110**, 533 (2009).
[16]X. Huang (NASA/Ames), personal communication (2016).
[17]A. Ben Reuven, Phys. Rev. **145**, 7 (1966).
[18]C. G. Gray and K. E. Gubbins, *Theory of Molecular Fluids* (Oxford University Press, Oxford, 1984).
[19]J. P. Bouanich, H. Aroui, S. Nouri, and A. Picard-Bersellini, J. Mol. Spectrosc. **206**, 104 (2001).
[20]M. D. Marshall, K. C. Izgi, and J. S. Muenter, J. Chem. Phys. **107**, 1037 (1997).
[21]M. Afzelius, P.-E. Bengtsson, and J. Bonamy, J. Chem. Phys. **120**, 8616 (2004).
[22]S. V. Ivanov, L. Nguyen, and J. Buldyreva, J. Mol. Spectrosc. **233**, 60 (2005).
[23]F. Thibault, L. Gomez, S. V. Ivanov, O. G. Buzykin, and C. Boulet, J. Quant. Spectrosc. Radiat. Transfer **113**, 1887 (2012) and references therein.
[24]Q. Ma, C. Boulet, and R. H. Tipping, J. Chem. Phys. **140**, 104304 (2014).
[25]Q. Ma, C. Boulet, and R. H. Tipping, J. Chem. Phys. **140**, 244301 (2014).
[26]C. Boulet, Q. Ma, and R. H. Tipping, J. Chem. Phys. **143**, 124313 (2015).
[27]L. R. Brown and D. B. Peterson, J. Mol. Spectrosc. **168**, 592 (1994).
[28]V. I. Starikov, Opt. Spectrosc. **114**, 15 (2013).
[29]M. R. Cherkasov, J. Quant. Spectrosc. Radiat. Transfer **141**, 73 (2014).
[30]M. R. Cherkasov, J. Quant. Spectrosc. Radiat. Transfer **141**, 89 (2014).
[31]S. Hadded, F. Thibault, P. M. Flaud, H. Aroui, and J. M. Hartmann, J. Chem. Phys. **120**, 217 (2004).